

DIAGNOSTIC TEST-BEAM-LINE FOR THE INJECTOR OF MESA*

I. Alexander[†], K. Aulenbacher

Institut für Kernphysik, Johannes Gutenberg-Universität, D-55099 Mainz, Germany

Abstract

With the test-beam-line it is possible to measure the two transverse phase-spaces and the temporal distribution of the electron bunches. It is also possible to investigate the emittance close to the source. The beam-line components will be introduced and a selection of the results will be presented.

INTRODUCTION

MESA will be a multi-turn Energy Recovery Linac (ERL) which can be operated in two different modes. An ERL Mode (105 MeV) or an External Beam (EB) Mode (155 MeV) [1]. The source will be a 100 kV dc photo gun which delivers polarized electrons with a current of 150 μ A and an unpolarized electron beam with a beam current of 1 mA in stage-1 and 10 mA in stage-2. The goal is to operate in c.w.-mode which means a bunch charge (Q_b) of 0.8 pC in stage-1 and 8 pC in stage-2. More details on the MESA project and the current status can be found in [1–3].

The task of the diagnostic test-beam-line is to determine if the photo electron source (*PES*) can deliver a smaller normalized emittance (ϵ_n) than the acceptance of the accelerator with a sufficient safety margin - for all Q_b - which requires that $\epsilon_n \leq 1 \mu\text{m}$. For the operation of MESA the source should be reliable and deliver a high extractable charge with a long lifetime.

Semiconductor photo-cathodes have some properties that should be taken into account. When excited with photon energies close to the band gap energy it is possible to create spin polarized electrons with circular polarized photons. However, when operating in this mode one suffers from low quantum efficiency (*QE*) and reduced cathode lifetime. If high currents, but no spin-polarization, are desired it is advantageous to use higher photon energies, since the *QE* is almost an order of magnitude larger and the lifetime is longer. At around 400 nm the photo-cathodes can have a *QE* of $10\% \triangleq 32^{\text{mA}}/\text{w}$. For higher photon energies not only the *QE* increases but also the thermal emittance does. This is because of the fact, that the stimulated electrons have not enough time to thermalize while they are traveling through the semiconductor and end up with a wider energy distribution. This additional energy spread gets transferred into larger transverse momenta which leads to a larger thermal emittance [4].

The source in the diagnostic test-beam-line has delivered 700 C [5] within one charge-lifetime at average currents exceeding 1 mA. The experiment needs average current of 1(10) mA corresponding to an extracted charge of

$3.6(36) \text{ C}/\text{h}$. Therefore, the transmission from *PES* to target should be as big as possible, to allow long continuous runtimes. To achieve this requirement a RF-synchronized laser must excite photo-emission. We will capture the so-produced bunches by a harmonic buncher system which can accept bunches with an extension of about 160° [6]. This leads to the requirement that the emitted intensity - which is the convolution of the temporal laser intensity profile and the response of the photo-cathode - must fit into this interval. Fractions outside the interval may be suppressed by a chopper system to provide very clean operating conditions for MESA. In the setup described here one of the circular deflecting cavities which were developed for the chopper system of MESA is used as temporal diagnostic instrument - see below.

COMPONENTS

Beam Line

A schematic overview of the beam-line setup is given in Fig. 1. In the upper left side there is the dc photo gun with a load-lock system and a potential of -100 kV . After the excitation of the electrons by laser light they are accelerated in the vertical direction. 1 m downstream of the source the first analyzing stage (scanner 1) is placed followed by an α -magnet which bends the electrons 270° from the vertical to the horizontal direction. Between the both α -magnets the second analyzing stage (scanner 2) is mounted. Here the evolution of ϵ_n with respect to the position of scanner 1 can be studied. If the second α -magnet is switched off investigations of the temporal distribution (*TD*) of the electron beam can be done with a deflecting cavity [7, 8] and a Ce:YAG screen. If the second α -magnet is switched on the electrons pass by the third analyzing stage (scanner 3) where it is possible to take a closer look to the beam halo with two perforated Ce:YAG screens. Behind scanner 3 there is a Wien-Filter for spin manipulation and a double scattering Mott polarimeter. This device is currently under test and promises to yield very precise polarization measurements [9] for the experiments (P2 [10] and MAGIX [11]) foreseen at MESA. It is, however, not relevant for the contents discussed here. All components between the source and the second α -magnet/scanner 3 are UHV compatible and bakeable. There are focusing elements like quadrupoles (blue) and solenoids (green) as well as several steering magnets which are not shown in Fig. 1.

The laser system (*LS*) for unpolarized high average electron current is installed close to the source chamber to create a minimized beam spot on the photo-cathode.

* Work supported by the German Science Foundation (DFG) under the Cluster of Excellence PRISMA

[†] alexand@kph.uni-mainz.de

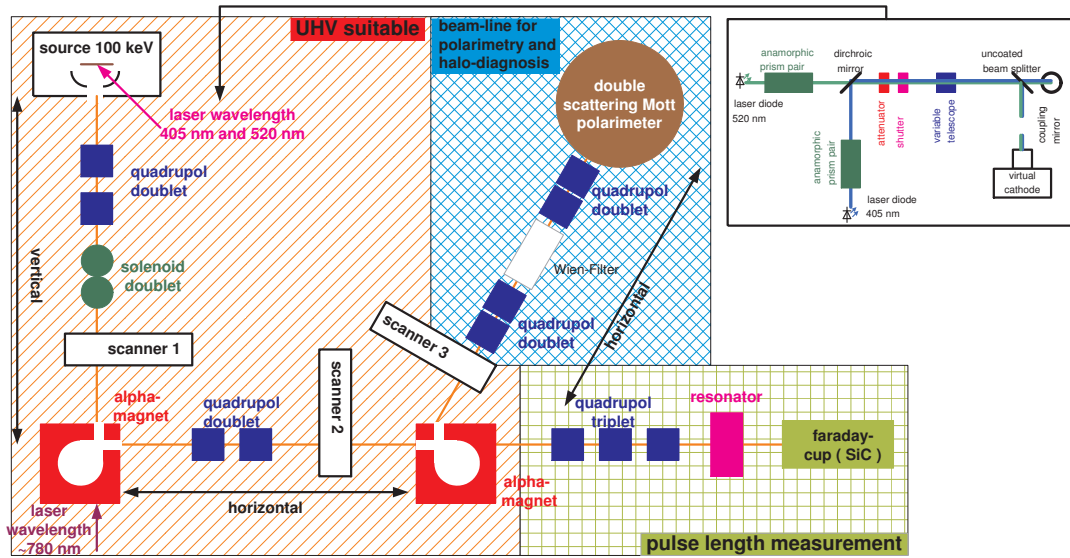


Figure 1: Schematic overview of the beam-line setup and the laser system (top right).

Laser System

The *LS* used for the presented results consists of two laser diodes (*LD*) with different wavelengths (λ_L) of 405 nm and 520 nm respectively and illuminates the cathode through a view-port on the bottom of the source chamber. A schematic sketch is illustrated in Fig. 1 (top right). At short distance after both *LDs* there is an anamorphic prism pair to compensate the astigmatism of the diodes. After the prism pair a dichroic mirror to combine both λ_L is installed, followed by a remotely controlled attenuator and shutter. The next element is a variable telescope to create different beam spot sizes (*BSS*) on the photo-cathode. The penultimate element is an uncoated beam splitter which couples out 3% of the laser power (P_L) and brings it onto a CCD-camera which works as virtual cathode to determine the *BSS* of the laser. The rest of P_L is reflected onto the photo-cathode via a mirror. An example of the laser spot shape at the waist is given in Fig. 2 for both λ_L . These 2D plots show the normalized intensity over the pixels of the camera which have a size of $6.6 \mu\text{m}$.

The irregular patterns (in particular of the green *LD*) in Fig. 2 and the temporal distribution (at aspired Q_b) presented below in Fig. 8 illustrate the inferiority of *LDs* in comparison to a dedicated *LS* such as fiber based MOPA's [12]. However, for our purposes, these lasers, which are cheap and reliable, are adequate.

The *LS* can be operated in c.w. or in pulse train mode (*PTM*). For both modes the injection current of the laser diode driver (*LDD*) is superimposed by a RF power (P_{RF}) of 1.7 W with $v_{RF} = 1.3 \text{ GHz}$. P_{RF} can be adjusted by an attenuator to optimize the operating parameters to different *LD* types. In *PTM* the *LDD* is supplied by rectangular shaped pulses with a length of $\tau \geq 300 \mu\text{s}$ and a repetition rate $v \geq 5 \text{ Hz}$ from a pulse generator. The *PTM* is used to minimize the thermal load on the screens with respect to

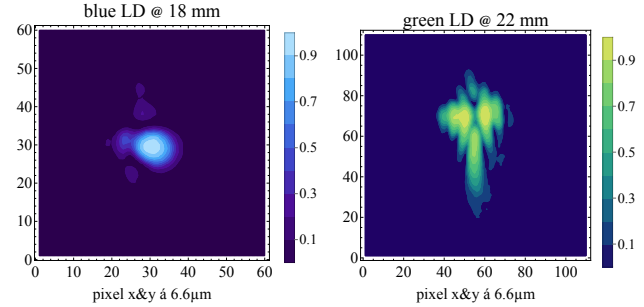


Figure 2: Examples for the normalized intensity of the *BSS* on the virtual cathode for the blue *LD* (left) and the green *LD* (right). In the plot title is also indicated the telescope setting.

high Q_b measurements. In the figures 5, 6 the Q_b is replaced by an equivalent average current which would occur in c.w. operation. Investigations with the deflecting cavity in the test-beam-line have clarified that the RF synchronized pulses within the pulse train are stable, which is depicted in Fig. 3. Here are taken four examples of the *TD* within a $300 \mu\text{s}$ long pulse train and it can be seen that the blue *LD* produces a double pulse with a RF phase length of $\vartheta_{RF,b} < 120^\circ$ (left) and the green *LD* generates single pulses with $\vartheta_{RF,g} < 100^\circ$ (right). Additional information on the *LS* can be found in [13].

The reason for the two different λ_L is to check the influence of it on ϵ_n and because both *LDs* show different pulsing behavior which are illustrated in Fig. 3 and thus, these measurements enables to consider the influence of the pulse shape on the ϵ_n growth for higher Q_b .

Scanner Devices

All three scanners have at least one Ce:YAG screen with a $\varnothing = 25 \text{ mm}$ to optimize the beam trajectory and to make

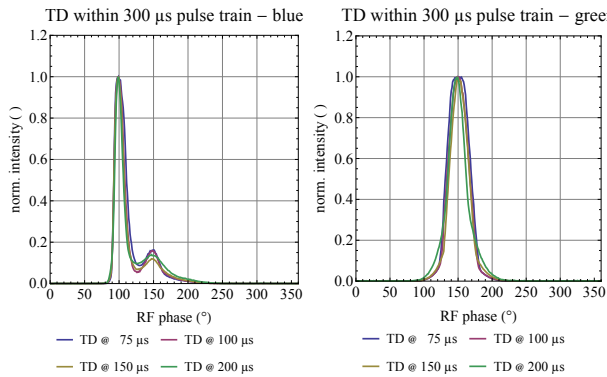


Figure 3: Examples for the RF synchronized pulses within a $300\mu\text{s}$ pulse train for the blue *LD* (left) and the green *LD* (right). Over 4σ of both distributions lie within $\vartheta_{RF} = 120^\circ$.

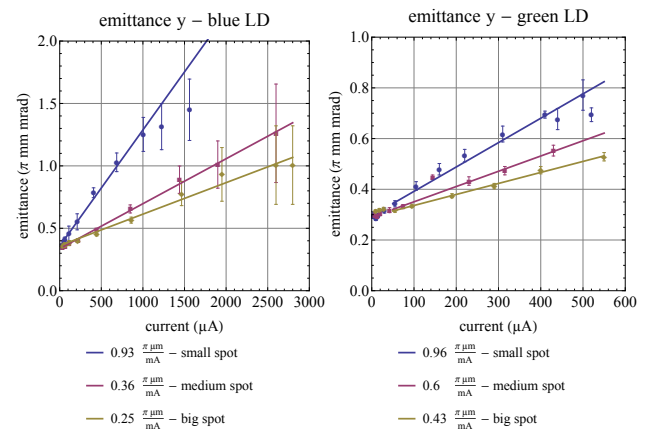


Figure 5: ϵ_n results from quad scan for the blue *LD* (left) and the green *LD* (right) plotted over I_e .

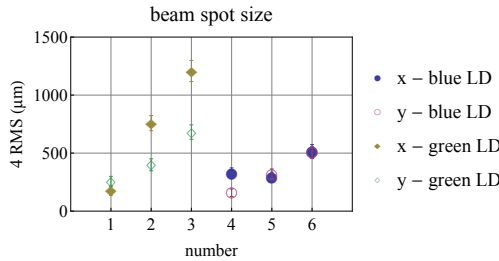


Figure 4: Overview of the *BSSs* generated by the telescope for small, medium and big laser spot.

emittance measurements by quadrupole scans. The electron facing side of the Ce:YAG screens is coated with *Al* to take the charge away and to avoid image distortion by charging of the surface. Scanner 1 and 2 also contain *W* wires with a $\varnothing = 40\mu\text{m}$ for emittance measurements and to investigate the halo distribution because of the higher dynamic range of a PMT-scintillator setup in comparison to a CCD-camera. Furthermore, scanner 1 has two slit arrays which are oriented perpendicular to each other. They have a slit width of $25\mu\text{m}$ and a spacing of $250\mu\text{m}$ to make emittance measurements complementary to quad scan results. In scanner 2 the slits are replaced by a hole mask (pepper pot) with 21×21 holes with a $\varnothing = 25\mu\text{m}$ and a spacing of $250\mu\text{m}$ in both directions. The purpose of scanner 3 is halo investigations and for that there are mounted two additional perforated Ce:YAG screens with a 2 mm or a 3 mm hole. Here the observing direction is the same as the incident electrons come from and thus, the screens are coated with *ITO* in addition.

RESULTS

Quad Scan

For the quad scan the focusing strength k of one quadrupole is varied in small steps and the beam profile is obtained from a Ce:YAG screen with a CCD-camera. The dimensions of the *BSSs* are shown in Fig. 4 and in Fig. 5 are presented some results of ϵ_n for the blue *LD* (left) and for the green one (right). The legends indicate the I_e de-

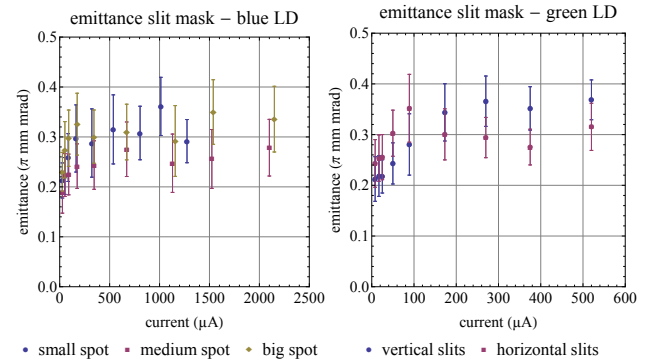


Figure 6: ϵ_n results from the slit mask measurements plotted over I_e for the blue *LD* (left) and the green *LD* (right).

pending slope of ϵ_n and the used *BSS*. These results clarify a dependence on the *BSS* and show that the requirements for MESA stage-1 could be fulfilled with the medium spot size for both *LDs*.

Slit Mask

In the slit mask emittance measurement method small slices of the beam are cut-out. With the width, the displacement and the amplitude of each beamlet it is possible to reconstruct the phase-space distribution. More details of the slit mask method can be seen in [14]. Furthermore, with these parameters ϵ_n can be calculated. In Fig. 6 are introduced some results for the blue *LD* (left) and for the green one (right). This data also represents the $1\sigma - \epsilon_n$.

If Fig. 5 and Fig. 6 are compared it strikes that the results for ϵ_n from the slit mask does not show a dependence on I_e for currents $> 100\mu\text{A}$ for both λ_L . The values scatter around $\epsilon_n \approx 0.3\pi\mu\text{m}$. This could be explained with the fact, that the phase-space distribution is curved with increasing I_e and if an ellipse is used to describe this distribution ϵ_n becomes larger to capture the same proportion of particles as in case of the slit mask. This should not be the case for the slit mask measurements which capture the true (conserved)

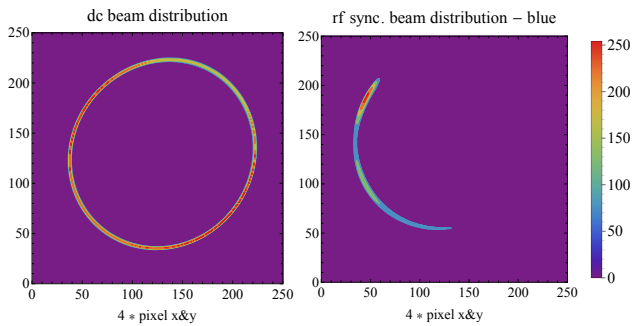


Figure 7: Example intensity distribution for a dc (left) and a c.w. (right) beam behind the deflecting cavity.

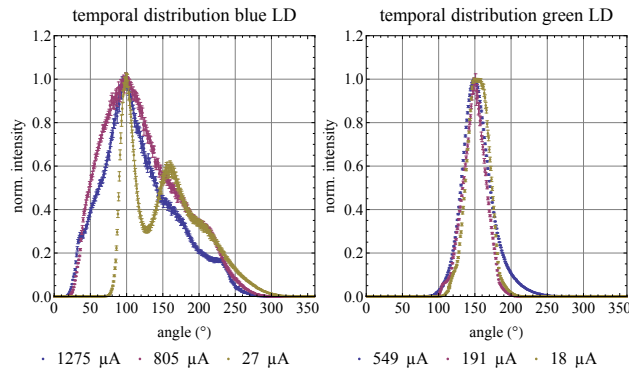


Figure 8: Selection of the I_e dependent evolution of the TD for the blue LD (left) and the green LD (right). The corresponding I_e is indicated in the legend.

emittance area. Our measurements (Fig. 6) seem to support this assumption.

Temporal Distribution

The deflecting cavity works with the MESA RF and is synchronized to the LS. Over the applied RF field in the cavity the beam is deflected circular and thus, the TD is transformed into a transverse one which can be observed with a CCD-camera and a Ce:YAG screen. The analyzed pictures are a superposition of many synchronous bunches and an example for a dc (left) and c.w. (right) beam of the blue LD is given in Fig. 7.

Due to the long drift space between the PES and the deflector (~ 4.5 m) strong modifications of the TD by space-charge can be expected. Investigations have been done for both λ_L and for different I_e up to the mA region. Fig. 8 is representing a selection of TDs for both LDs and the

corresponding I_e are indicated in the legends. The LDs used here are an easy means to demonstrate the performance of the analysis systems at the relevant Q_b for MESA.

SUMMARY

The collected experience with the diagnostic test-beam-line have shown that it is a powerful tool to investigate the transverse ϵ_n and the TD for different bunch shapes up to the mA (~ 1 pC/bunch) region. Investigations of the two transverse phase-spaces with quadrupole scan technique and the determination of the beam profile with a screen or with wires are possible. The beam-line gives the possibility of a cross check between quad scan and slit mask measurements.

The test-beam-line setup has a similar length compared to the one foreseen for MESA, where the necessities of spin manipulation increase the size by about 1.5 m. The presented results indicate that MESA stage-1 parameters can be achieved, whereas stage-2 parameters probably require a shorter distance between PES and injector (at the expense of spin manipulation flexibility) and/or a PES with larger accelerating gradient and potential.

REFERENCES

- [1] R. Heine, ERL2015, Stony Brook, USA, WEIBLH1049
- [2] T. Stengler, K. Aulenbacher et al., IPAC'16, Busan, Korea, WEPMB009
- [3] R. Heine, K. Aulenbacher et al., IPAC'16, Busan, Korea, TUPOW002
- [4] I. V. Bazarov, Journal Of Applied Physics 103, 054901 (2008)
- [5] K. Aulenbacher, I. Alexander et al., J. Phys. Conf. Series 298 (2011) 012019
- [6] P. Heil, Diploma thesis, JGU Mainz, Germany (2015)
- [7] V. Bechthold, Diploma thesis, JGU Mainz, Germany (2013)
- [8] B. Ledroit, Bachelor thesis, JGU Mainz, Germany (2014)
- [9] A. Gellrich, J. Kessler, Phys. Rev. A 43, 204 (1991)
- [10] N. Berger, K. Aulenbacher et al., PhiPsi15, USTC, China (2015)
- [11] A. Denig, APS April Meeting (2015), Baltimore, USA
- [12] D. G. Ouzounov et al., PAC07, Albuquerque, USA, MPOAS044
- [13] I. Alexander, K. Aulenbacher et al., ERL2015, Stony Brook, USA, THIALH2069
- [14] M. Zhang, FERMILAB-TM (1988)